Large magnetothermopower and anomalous Nernst effect in $HfTe_5$

Junfeng Hu,[1,2] Marco Caputo,[3] Eduardo Bonini Guedes,[2,3] Sa Tu,[1] Edoardo Martino,[2] Arnaud Magrez,[2] Helmuth Berger,[2] J. Hugo Dil,[2,3] Haiming Yu,[1,*] and Jean-Philippe Ansermet[2,†]

[1]*Fert Beijing Institute, BDBC, School of Microelectronics, Beihang University, Xueyuan Road 37, Beijing 100191, China*

[2]*Institute of Physics, station 3, Ecole Polytechnique Fédérale de Lausanne, 1015 Lausanne-EPFL, Switzerland*

[3]*Photon Science Department, Paul Scherrer Institute, CH-5232 Villigen PSI, Switzerland*

(Received 20 June 2019; published 12 September 2019)

Topological quantum materials have stimulated growing attention because they reveal novel aspects of condensed matter physics and point to new opportunities in materials science, in particular for thermoelectrics. Here, we experimentally study thermoelectric effects in $HfTe_5$, which was predicted to be at the boundary between strong and weak topological insulators. The magnetic field dependence of $HfTe_5$ thermoelectric properties attests to the anomalous character of this material, supported by our angle-resolved photoemission spectroscopy (ARPES) measurements. At 36 K, the thermopower of -277 μV/K is reached when a field of 0.4 Tesla is applied, while it is -157 μV/K at zero field and a large Nernst coefficient up to 600 μV/K is observed at 100 K with magnetic field of 4 T. A possible topologically nontrivial band structure is proposed to account for our observations. Our results constitute a highly constraining set of data for any model of transport based on $HfTe_5$ band structure. Furthermore, the extraordinary thermoelectric properties suggest a new paradigm for the development of thermoelectric applications based on layered transition-metal chalcogenides.

DOI: 10.1103/PhysRevB.100.115201

I. INTRODUCTION

In the field of topological quantum materials [1,2] a great deal of attention has been paid to Dirac/Weyl semimetals such as TaAs [3,4], Cd_3As_2 [5,6], and Na_3Bi [7,8]. In Dirac/Weyl semimetals, the chiral anomaly is one of the typical features [9]. Experimental efforts have been focusing on observing these chiral effects. For instance, a negative longitudinal magnetoresistance (LMR) was observed in Weyl semimetals when an external magnetic field was applied parallel to electrical field, i.e., $B \parallel E$ [10]. However, also many trivial effects can explain a negative longitudinal magnetoresistance and it cannot be directly interpreted as evidence for a chiral anomaly. An alternative signature of the chiral anomaly was found in the thermoelectric properties in Cd_3As_2 studied by Jia *et al.* [5], showing that this approach bears more promise. Very recently, a new heat-transport mechanism called chiral zero sound has been predicted in Weyl semimetals [11] and could be used to explain the observed giant thermal conductivity in Weyl semimetal TaAs [12] and anomalous heat current in GdPtBi [13]. Here, we report our systematic study of the thermoelectric properties (both Seebeck and Nernst effects) of layered Hafnium pentatelluride ($HfTe_5$) single crystals and show that the observed results are consistent with a nontrivial electronic structure.

$HfTe_5$ single crystals were first synthesized in 1973 [14]. It crystallizes in an orthorhombic structure [see Fig. 1(a)] with space group *Cmcm*. The trigonal prismatic chains of $HfTe_3$ are along the *c* axis and the parallel zigzag chains of Te_2 are along the *a* axis when considering a two-dimensional slice of $HfTe_5$ normal to the *b* axis. Figure 1(b) shows the corresponding 3D Brillouin zone (BZ) [15]. A peak anomaly of the electric resistivity in the temperature range from 40 K to 80 K has been observed by different groups [16–20]. The seminal work by Jones *et al.* [18] showed that the Seebeck coefficient changes sign at about 85 K, which they interpreted as a change of charge carrier type, from electronlike (EL) to holelike (HL). Recently, in $HfTe_5$ single crystals, Kumar *et al.* [19] observed a large out-of-plane transverse magnetoresistance of up to 9000% at 9 T and a linear in-plane magnetoresistance, while Wang *et al.* [21] detected a negative LMR which they ascribed to a chiral anomaly and Niemann *et al.* [22] show vanishing magnetothermoelectric transport at low temperatures. $HfTe_5$ and its cousin material $ZrTe_5$ were predicted to be at the boundary between weak and strong topological insulators by an ab initio study [23] and were subsequently studied by angle-resolved photoemission spectroscopy (ARPES) [15,17,24,25]. Although $ZrTe_5$ has been demonstrated as showing a chiral magnetic effect [10] and a large Berry curvature-induced anomalous Hall effect [26], experimental confirmation of the topological properties of $HfTe_5$ is still pending.

Thermoelectric properties depend on the energy derivative of the conductivity, according to the Mott relations. Therefore, their study constitutes a strong test for chiral anomaly and topological properties [5,6]. For example, large Nernst coefficients were predicted and found in various materials [27,28], with an extremely large value in the Weyl semimetal NbP [29]. Some groups have also studied electric transport in nanothick $ZrTe_5$ flakes to explore the dimensionality of the conductance [30]. The anomalous transport properties and quasi 2D Dirac semimetal description of $ZrTe_5$ has been

*haiming.yu@buaa.edu.cn

†jean-philippe.ansermet@epfl.ch

 ©2019 American Physical Society

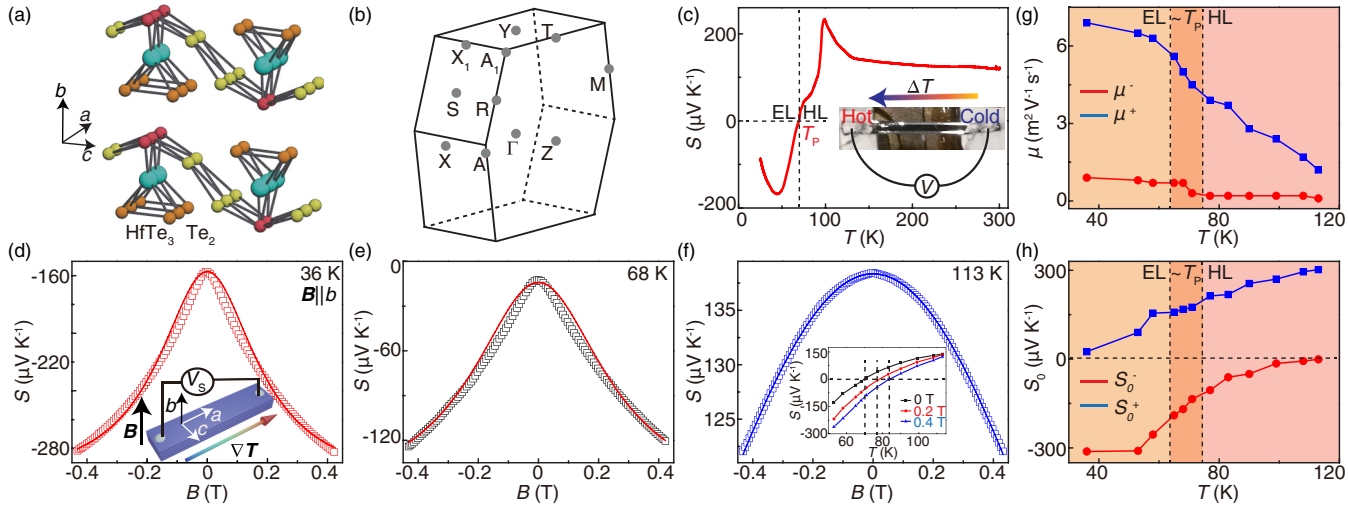

FIG. 1. (a) and (b) are the crystal structure and 3D Brillouin zone of $HfTe_5$, respectively. (c) The transition temperature T_p is found to be around 70 K. Inset: photo of the sample resting on top of a heater on one side (hot) and a copper block on the other side (cold). Seebeck coefficients as a function of magnetic field applied along the b axis at (d) 36 K, electronlike, below T_p. (e) 68 K, around T_p. (f) 113 K, holelike, above T_p. The lines in (d), (e), and (f) are fitting curves using Eqs. (2) and (3). Inset of (f): temperature dependence of the Seebeck coefficient measured at 0, 0.2, and 0.4 T. The data are extracted from data in Fig. S3. The fitting parameters: mobilities and Seebeck coefficients are shown in (g) and (h), respectively. Data obtained with sample A.

reported by Martino *et al.* [31] very recently. In this work, we present magneto-thermopower and Nernst effect measurements on bulk 3D $HfTe_5$ single crystals. We find a very large change in the Seebeck coefficient, about 140 μV/K at 53 K, when a mere 0.4 T magnetic field is applied along the b axis, i.e. normal to the layers. Furthermore, we find an extraordinarily large value of the Nernst effect, more than 120 μV/K at 100 K in a field of 0.4 T and reaching an astonishing 600 μV/K at 4 T.

II. RESULTS

Results obtained with different samples were consistent with one another. In particular, the thermoelectric properties had special features at fields and temperatures at which electrical transport properties also presented special features. Our paper is structured as follows: First we present our magnetothermopower (MTEP) observations with magnetic field along the b axis, i.e., perpendicular to the temperature gradient. Second, the longitudinal MTEP, i.e., with field parallel to the temperature gradient. Third, we report on the Nernst effect (ANE) at high magnetic fields for several temperatures. Fourth, we report on low-field ANE measurements and analyze the data with a two-band model. Finally, we present our ARPES measurements of the temperature-dependent electronic structure. We use magnetoresistance and Hall measurements to confirm the quality of our crystals and the results are shown in the Supplemental Material [32].

Figure 1(c) shows the Seebeck coefficient of sample A (see sample information in the Supplemental Material), measured as a function of temperature in the range from 25 K to 300 K at zero magnetic field. When the crystal is cooled down starting from room temperature, the Seebeck coefficient S increases slightly until 130 K is reached, and then increases sharply, reaching a maximum of 234 μV/K at around 100 K. Below 100 K, S decreases rapidly with decreasing temperature and crosses zero around 70 K (defined as the transition temperature T_p), and continues to decrease down to $-168\,\mu$V/K at 44 K and increase again with temperature further down to 25 K. This sign change has also been observed in the pioneering work of Jones *et al.* [18] They attributed it to a change of majority charge carrier from HL to EL carriers. In this model, the total thermopower S is a weighted sum of EL($-$) and HL($+$) Seebeck coefficients [33],

$$S = \frac{\sigma_- S_- + \sigma_+ S_+}{\sigma_- + \sigma_+} \tag{1}$$

where S_-, S_+ and σ_-, σ_+ are the Seebeck coefficients and conductivities of EL and HL channels, respectively. At the transition temperature T_p where the thermopower changes sign, the contributions from both channels cancel out, resulting in a nearly zero thermopower [see also Fig. S1(a)]. Except for the sign change of the Seebeck coefficient at the transition temperature T_p, the rapid change of the Seebeck coefficient around T_p is also quite interesting and needs to be understood. A simple explanation for this is that the temperature change induces a sharp or discontinuous change of the density of states near the Fermi level (as indicated in Fig. 6), which could result in a drastic change of the energy derivative of the conductivity and therefore, lead to a larger Seebeck coefficient.

The thermopower was measured at different temperatures as a function of the magnetic field applied along the b axis [Fig. 1(d) inset]. The MTEP $\Delta S = S(B) - S(0)$ [34] is quite large, as shown in Figs. 1(d), 1(e) and 1(f). At 68 K [Fig. 1(e)], the Seebeck coefficient changes from around -12.6 μV/K at zero magnetic field to as much as -122.5 μV/K at the relatively small magnetic field of 422 mT. The thermopower has been measured at the transition temperature also on sample D, where the thermopower changed from less than 0.1 μV/K at zero magnetic field to as much as -100 μV/K at 422 mT [Fig. S1(b)]. Large anisotropies exist along different

crystallographic orientations due to the layered structure of $HfTe_5$, and the field orientation-dependent thermopowers are shown in Fig. S2.

In the semiclassical regime, the Seebeck and Nernst coefficients can be calculated with the Mott formula [35,36]. We adapt Eq. (1) by using the empirical Eq. (2) used to describe magnetoresistance [21]. This leads to the following two-band model for the Seebeck coefficient when the magnetic field is along the b axis,

$$\sigma^{\pm}(B) = \sigma_0^{\pm}\frac{1}{1+(\mu^{\pm})^2B^2} \tag{2}$$

$$S(B) = \frac{\sigma^-(B)S_0^- + \sigma^+(B)S_0^+}{\sigma^-(B)+\sigma^+(B)} \tag{3}$$

where σ_0^- and σ_0^+ are the EL and HL conductivities at zero field, S_0^- and S_0^+ the Seebeck contributions from EL conductivity and HL conductivity, and $\mu^{\pm}$ the mobilities of both charge carriers. The red line in Fig. 1(e) is the best-fitting curve obtained using $S_0^- = -169\ \mu V/K$, $S_0^+ = +168\ \mu V/K$, $\mu^- = 0.7\ m^2\ V^{-1}\ s^{-1}$, and $\mu^+ = 5\ m^2\ V^{-1}\ s^{-1}$ and attributing almost half the measured conductivity to each channel ($\sigma_0^- = 180\ \Omega^{-1}\ cm^{-1}$ and $\sigma_0^+ = 153\ \Omega^{-1}\ cm^{-1}$). The total conductivity extracted from the resistance measurements shown in Fig. S3 around T_p at zero magnetic field is $\sigma = \sigma_0^- + \sigma_0^+ = 333\ \Omega^{-1}\ cm^{-1}$, which is fairly close to the value given by Zhao *et al.* [20]. As there are six parameters to adjust, it is not surprising to account for the data using reasonable values for every one of them, but we noticed that this empirical two-band model fails to reproduce the concavity of the experimental data in the lowest field range, no matter how we try to set the fitting parameters. Keeping the conductivity unchanged, we also fitted our data at different temperatures by changing the mobilities [Fig. 1(g)] and the Seebeck coefficients [Fig. 1(h)]. Figures 1(d) and 1(f) are two of the selected temperatures, namely, above and below the transition temperature.

In order to further characterize the large MTEP, we measured it at different temperatures around T_p, from 36 K to 172 K [Fig. S4(a)]. From these data we extracted the temperature dependence of the Seebeck coefficient at applied fields of 0, 0.2, and 0.4 T [Fig. 1(f) inset]. Thus, we find that the temperature dependence of the Seebeck coefficient is strongly modified when applying an external field. In particular, the temperature T_p is changed by applying a magnetic field, varying from 70 K (zero field) to 84 K (0.4 T) in sample A. This might be attributed to a magnetic field-induced change of the carrier mobility. This assumption is in sharp contrast with the conventional behavior of a two-band model.

Let us now focus on the longitudinal field configuration ($B \parallel a$), i.e., the field is applied along the temperature gradient direction (Fig. 2, sample B). At temperatures below T_p, the EL Seebeck contribution dominates since a negative Seebeck coefficient is observed [Fig. 2(a)]. When the temperature is above T_p, e.g., around 120 K, the thermopower is positive and its magnetic dependence shows a small positive increase with field, as shown in Fig. 2(b). Both below and above the transition temperature T_p, the magnetothermopower is not very large, namely -18.5% for EL conductance at 30 K and 0.4% for HL conductance at 120 K. Whereas the magnetic

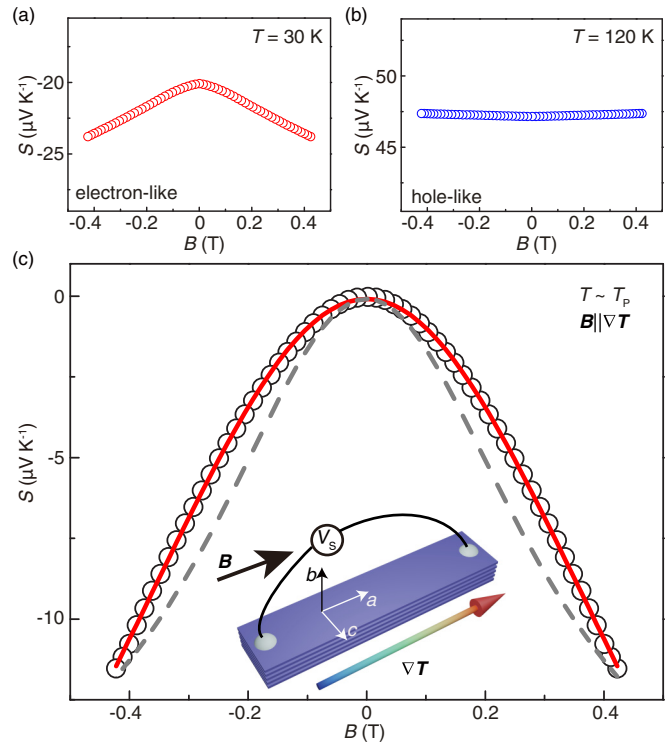

FIG. 2. (a) 30 K, electronlike, below T_p. (b) 120 K, holelike, above T_p. (c) 56 K, around T_p. The red line in (c) is a fitting using Eqs. (1) and (4) with $\beta^- = +1$ and $\beta^+ = -1$. The gray dashed line is a fitting with both β^- and β^+ equal to $+1$. Inset: measurement configuration. Data obtained with sample B.

field dependence is weak, the Seebeck coefficients themselves are sizable, about $-23\ \mu V/K$ (EL) and $47\ \mu V/K$ (HL).

Surprising results occur around the transition temperature T_p ($T_p = 56$ K in sample B). T_p is sample dependent because it depends strongly on doping, stress, and pressure [37]. The thermopower at zero magnetic field vanishes, but the magnetic field-dependent contribution to the thermopower is rather large as shown in Fig. 2(c). A field of 0.4 T, which is relatively small for a nonmagnetic solid, can easily break the balance of EL and HL contributions [Eq. (1)] and create a thermopower as large as $-11.4\ \mu V/K$. The thermopower in the longitudinal configuration ($B \parallel \nabla T \parallel a$, Fig. 2) cannot be accounted for by a one-band model [5,38,39]. As we have discussed above, the sign change of the thermopower is one piece of evidence that two types of charge carriers are present in $HfTe_5$ near T_p. The anomalous resistivity peak [Fig. S3(a)] is another indication that, around the transition temperature, both EL and HL carriers contribute [20]. Therefore, a two-band model needs to be considered once again to account for the longitudinal MTEP near T_p. We adapt a general formula for describing negative LMR with chiral anomaly in Weyl semimetal which was used by Huang *et al.* [39] and expand it to a two-band model,

$$\sigma_{Lxx} = \sigma_{Lxx0}^-(1+\beta^-(\mu^-)^2B^2) + \sigma_{Lxx0}^+(1+\beta^+(\mu^+)^2B^2) \tag{4}$$

where $\beta^{\pm} = \pm 1$. We assume the EL and HL conductivities σ_{Lxx0}^- and σ_{Lxx0}^+ to be field independent, which is especially

likely at the low field values considered here (the experimental data shown in Figs. S3 and S5 indicate the MR is only 0.3% at 0.4 T).

The results shown in Fig. 2(c) can be accounted for by Eqs. (1) and (4) with fitting parameters $\sigma^{-}_{Lxx0} = 224\ \Omega^{-1}\,\mathrm{cm}^{-1}$ and $\sigma^{+}_{Lxx0} = 109\ \Omega^{-1}\,\mathrm{cm}^{-1}$, the sum of which is the experimental value of 333 $\Omega^{-1}\,\mathrm{cm}^{-1}$. The ratio $\sigma^{-}_{Lxx0}/\sigma^{+}_{Lxx0} \sim 2.1$ is very close to the residual-resistance ratio of 2.5 deduced from our measured data at 1.8 K and 300 K, when conduction is dominated by electrons at 1.8 K (EL) and holes at 300 K (HL). S_{-} and S_{+} are taken as the zero-field experimental results at temperatures far from T_{p}. Interestingly, when tuning the parameters in order to fit the large MTEP at T_{p} shown in Fig. 2(c), a positive β^{-} and a negative β^{+} provides an almost perfect fit [red line in Fig. 2(c)] when $\mu^{-} = 2.1\ \mathrm{m}^2\,\mathrm{V}^{-1}\,\mathrm{s}^{-1}$ and $\mu^{+} = 1.2\ \mathrm{m}^2\,\mathrm{V}^{-1}\,\mathrm{s}^{-1}$. If both β^{-} and β^{+} are forced to be positive, the fitting becomes very difficult and the best attempt is shown as the gray dashed line in Fig. 2(c). This result is again inconsistent with a simple conventional two-band model. The possible topological mechanism is that when a magnetic field is applied parallel to the temperature gradient direction for the longitudinal magnetothermopower measurements, the magnetic field breaks the time reversal symmetry and splits the Dirac node into two Weyl nodes along the field direction, which give rise to the two different effective quantum magnetic field [40,41].

As $1/\mu^{-}$ has units of T, it can be considered as an effective field $B_0^{-} = 1/\mu^{-} \sim 0.48$ T. The effective field B_0^{+} is found to be slightly larger than B_0^{-}, about 0.83 T. Such an effective field may be expressed as $B_0 = \sqrt{3\tau/\tau_i}B_{\mathrm{q}}$ where $B_{\mathrm{q}} = \frac{2E_F^2}{3e}\hbar v_F^2$ represents an effective quantum magnetic field induced by massless Dirac fermions in $HfTe_5$ [5]. Based on this analysis, the difference in the extracted values for B_0^{+} and B_0^{-} may originate from two possible mechanisms. First, the EL conductance and HL conductance may have different ratio of τ/τ_i (τ is the mean free time and τ_i is the intervalley scattering time). Second, the quantum magnetic field B_{q} may have different values for EL and HL conductances. This would be an indication that two types of massless Dirac fermions contribute to transport. In any case, we find that when the field is applied in the plane in which transport takes place, that is, when the classical Lorentz force is irrelevant, we find that the MTEP $\Delta S = S(B) - S(0)$ is of the order of magnitude of the Seebeck coefficient of many materials, even when the applied field is only 0.4 T. Furthermore, we find that by changing the direction of the applied magnetic field from the b axis to the a axis, we change completely the mobilities, for example, at around transition temperature, the ratio of which being $\mu^{-}/\mu^{+} = 1.7$ when the field is applied along the a axis whereas it is about $\mu^{-}/\mu^{+} = 0.14$ when the field is applied along the b axis.

The Nernst effect can be considered as a transverse Seebeck effect [36]. Figure 3(a) shows the schematic diagram for Nernst effect measurements. The Nernst coefficient N is determined as the ratio of the electric field in the c direction to the temperature gradient in the a direction. When the temperature is above T_{p}, the HL conductance dominates the transport as indicated by the temperature dependence of the Seebeck coefficient. Surprisingly, we find an astoundingly large Nernst

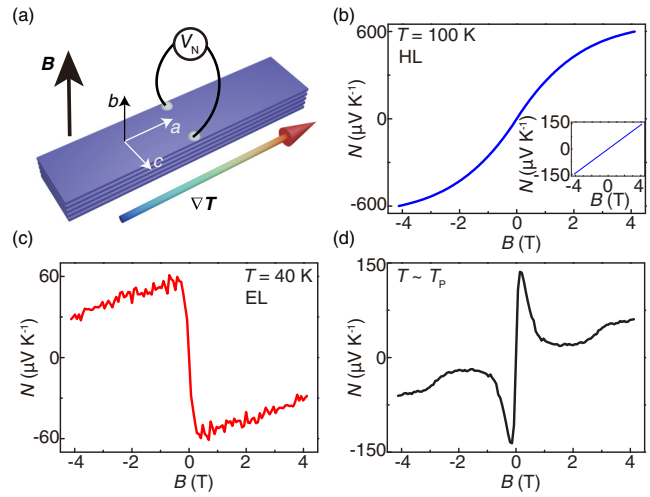

FIG. 3. (a) Schematic of Nernst effect measurement. (b) Holelike Nernst coefficient measured as a function of magnetic field at 100 K (above T_{p}). Inset: measurement at 130 K. (c) Electronlike Nernst coefficient measured at 40 K (below T_{p}). (d) Nernst coefficient measured at 70 K (near T_{p}). Data obtained with sample C.

coefficient [see Fig. 3(b)], reaching 600 μV/K at 100 K in a magnetic field of 4 T. As an asymptote is not reached, a larger Nernst coefficient can be expected if the magnetic field were increased further. Increasing the temperature from 100 K to 130 K, the steplike field dependence turns into a linear one [Fig. 3(b) inset]. While this field dependence is expected in a conventional material, the value remains very large [inset of Fig. 3(b)]. Below the transition temperature T_{p}, the Nernst effect presents a large steplike field dependence [Fig. 3(c)], the sharpness of which resembles the anomalous Nernst effect (ANE) of ferromagnetic thin films [42]. The ANE responses observed in ferromagnets are usually quite sharp because the field range over which the magnetization switches is narrow. To the contrary, a typical field value which is sufficient to saturate the ANE in a topological system is quite large, e.g., about 1 T for Cd_3As_2 [6]. It is yet another remarkable feature of $HfTe_5$ that it takes a relatively small field (0.18 T) to reach a plateau of the ANE, which might be an indication that the Berry curvature plays an important role in our samples.

Around the transition temperature T_{p} (70 K), a peculiar field dependence is observed as shown in Fig. 3(d): A sharp anomalous Nernst curve is observed with broad features at high fields. More data plots at other temperatures are shown in Fig. S6. One common feature of all our Nernst measurements is that the Nernst coefficient vanishes when the magnetic field tends to zero. This behavior is similar to that observed for Cd_3As_2 [5,6]. It has been theoretically studied by Sharma *et al.* [43] and interpreted as the Nernst effect of Dirac semimetals, where the effect is dominated by the anomalous contribution rather than the conventional contribution.

For a given magnetic field direction, the Nernst coefficient of sample C changed sign when going from above to below T_{p} (Fig. 3). The same sign change was found using sample A in which the temperature T_{p} is about 70 K [Figs. 4(a)–4(c)]. An anomalous Nernst coefficient as large as 87 μV/K was measured at 83 K in a field of 0.18 T and a linear field

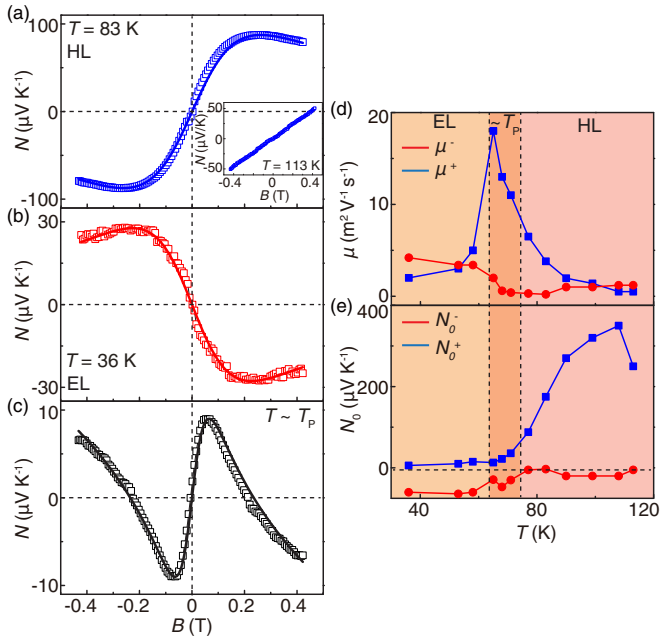

FIG. 4. (a) Holelike Nernst coefficient measured at 83 K (above T_p, inset: results at 113 K). (b) Electronlike Nernst coefficient measured as a function of magnetic field at 36 K (below T_p). (c) Nernst coefficient measured at 68 K (near T_p). (d) Mobilities μ^- (red dots) and μ^+ (blue squares) deduced from Nernst measurements, as a function of temperature. (e) Nernst parameters N_0^- (red dots) and N_0^+ (blue squares) deduced from Nernst measurements, as a function of temperature. Data obtained with sample A.

dependence was observed at temperatures above 113 K [inset of Fig. 4(a)]. More data plots at other temperatures are shown in Fig. S4(b). In order to analyze these Nernst data, we use Mott relations [35,44], which can be summarized in tensor form as:

$$\tilde{S} = \tilde{\rho}\frac{d\tilde{\sigma}}{dE_F}\frac{\pi^2 k_B^2 T}{3e} \tag{5}$$

From Eq. (5), we can derive the Nernst coefficient N as

$$N = S_{xy} = [\rho_{xx}\sigma'_{xy}(E_F) + \rho_{xy}\sigma'_{yy}(E_F)]\frac{\pi^2 k_B^2 T}{3e} \tag{6}$$

where the ρ_{xx} and ρ_{xy} are the resistivities, and $\sigma'_{xy}(E_F)$ and $\sigma'_{yy}(E_F)$ are the energy derivative of the electrical conductivities. In order to apply a two-band Hall model, we adapt the empirical formula for the magnetic-field dependence of the conductivity which has been applied successfully by others to account for their Hall measurements [45–47],

$$\sigma_{xy} = \sigma_{xy0}^- \frac{\mu^- B}{1+(\mu^-)^2 B^2} + \sigma_{xy0}^+ \frac{\mu^+ B}{1+(\mu^+)^2 B^2} \tag{7}$$

where $\sigma_{xy0}^- = n_- e\mu^-$ and $\sigma_{xy0}^+ = n_+ e\mu^+$ are electron and hole conductivities (n_- and n_+ are carrier concentrations for EL and HL band, respectively). By taking the energy derivative of the electrical conductivity σ_{xy} at the Fermi level, one can get:

$$\sigma'_{xy}(E_F) = \frac{d\sigma_{xy0}^-}{dE_F}\frac{\mu^- B}{1+(\mu^-)^2 B^2} + \frac{d\sigma_{xy0}^+}{dE_F}\frac{\mu^+ B}{1+(\mu^+)^2 B^2}. \tag{8}$$

Similarly, we deduce the energy derivative $\sigma'_{yy}(E_F)$ by using the empirical equation for magnetoresistivity σ_{yy} [Eq. (2) with $B \parallel b$]. Since the Nernst coefficient magnetic-field dependence is antisymmetric and becomes zero at zero field, while the $\sigma'_{yy}(E_F)$ gives a symmetrical contribution to the Nernst signal, $\sigma'_{yy}(E_F)$ can be ignored. Thus, we obtain a simplified two-band model for the Nernst coefficient as

$$N = N_0^- \frac{\mu^- B}{1+(\mu^-)^2 B^2} + N_0^+ \frac{\mu^+ B}{1+(\mu^+)^2 B^2} \tag{9}$$

where $N_0^- = \rho_{xx}\frac{d\sigma_{xy0}^-}{dE_F}\frac{\pi^2 k_B^2 T}{3e}$ and $N_0^+ = \rho_{xx}\frac{d\sigma_{xy0}^+}{dE_F}\frac{\pi^2 k_B^2 T}{3e}$ are the Nernst contributions from EL and HL bands.

This two-band model may be used to fit [lines in Fig. 4(a)–4(c)] the experimental data [dots in Figs. 4(a)–4(c)]. The fits require a temperature dependence of the four fitting parameters, namely μ^-, μ^+, N_0^-, and N_0^+, as plotted in Figs. 4(d) and 4(e). The mobilities μ^- and μ^+ thus deduced exhibit very different temperature dependences from what was obtained when fitting the magnetothermopower data (Fig. 1). Here, the holelike mobility μ^+ presents a maximum around T_p, instead of the steplike decrease deduced from the magnetothermopower. The electronlike mobility μ^- shows a moderate steplike drop around T_p, consistent with what was obtained from the magnetothermopower. Below T_p, the Nernst parameter for EL conductance N_0^- shows a much larger amplitude than N_0^+, whereas at temperatures well above T_p, the HL conductance N_0^+ becomes much larger than its EL counterpart N_0^- [Fig. 4(e)]. This is consistent with the assumption that at T_p, a transition occurs from EL to HL conduction, as first studied by Jones *et al.* [18]. However, the unconventional behaviors of hole mobility, its inconsistency with the magnetothermopower, and large Nernst coefficient of the hole band could not be accounted for by this simplified two-band model. Thus, a nontrivial band structure arising from topological properties, resulting in a strong Berry curvature, needs to be considered in order to account for the anomalous transport properties we observed in $HfTe_5$.

We gained further insight into the thermoelectric transport properties of $HfTe_5$ by measuring the electronic structure with ARPES, using sample E. From the measured data [see Fig. 5(a)], it can be deduced that the top of the valence band is not just a simple parabola, but rather an M-shaped band, whose maxima are slightly away from the Gamma point. This electronic structure is consistent with a nontrivial band structure or a large Berry curvature.

The temperature-dependent data show an upshift of the whole band structure (downshift of the chemical potential) by lowering the temperature: While at 120 K the Fermi level touches the very tip of the valence band, at 40 K the Fermi level cuts the valence band, showing a sizable Fermi momentum. In Fig. 5(b) this trend is clearly shown using momentum distribution curves (MDCs) at a fixed binding energy (350 meV) for different temperatures. Here, two effects are visible; first, the peak at -0.1 Å^{-1} shifts away from the Gamma point, which is exactly what would be expected for a holelike band moving to lower binding energy. Furthermore, a new feature increases in intensity around -0.4 Å^{-1},

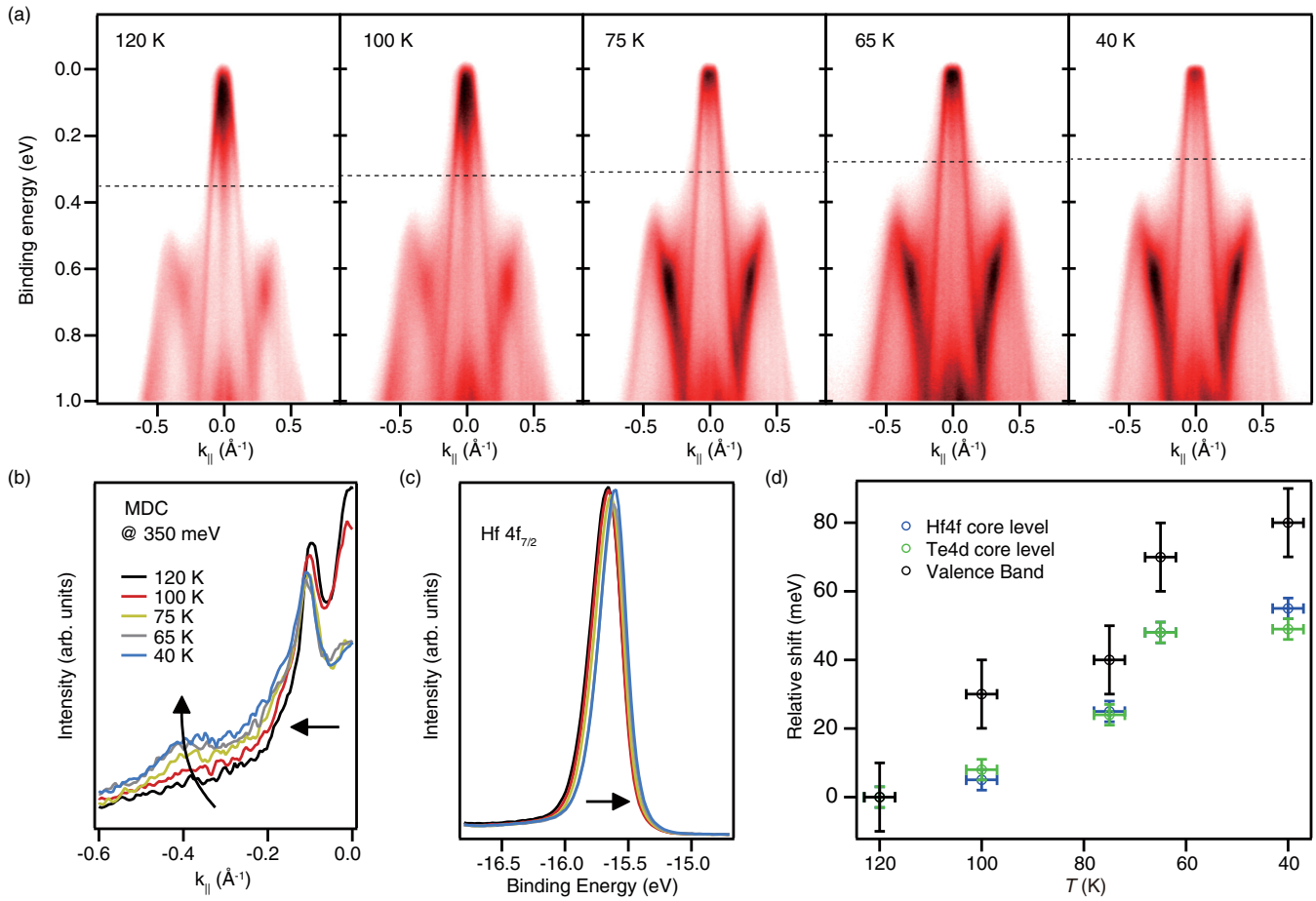

FIG. 5. (a) Temperature evolution of the band structures in $HfTe_5$ along the Y-Γ-Y direction. The dashed horizontal lines indicate the energy for which identical MDC peak positions are obtained. (b) A momentum distribution curve at a fixed binding energy of 350 meV for all the temperatures. (c) Hf $4f_7/2$ core level as a function of temperature, the color legend is the same as in (b). (d) Summary of all the observed shifts with 120 K data as a reference. Data obtained with sample E.

corresponding to the appearance of a second holelike band also shifting towards lower binding energy. The ARPES data also show a significant change in intensity of a feature around the Gamma point visible both in Figs. 5(a) and 5(b). This is probably related to the finite angular resolution along the direction perpendicular to the band map and a slight misalignment ($<0.1^\circ$) of the sample which changes with temperature. The feature itself is located at finite momentum and looks like incoherent spectral weight often found cascading down from band minima, providing a further indication of strong deviations from a simple holelike dispersion, also visible in Fig. S7. In combination with the steep dispersion, this results in a drastic change of intensity, which, however, does not affect our general interpretation. The shift of the electronic structure towards lower binding energies with decreasing temperature is also visible in the core level spectra. Figure 5(c) shows the Hf $4f_{7/2}$ core level component as a function of temperature, in which a clear monotonic shift toward lower binding energy is visible. To summarize, ARPES shows a clear shift of the chemical potential with increasing temperature, which, given the peculiar dispersion around the valence band maximum, results in a Lisfshitz-type transition, with the chemical potential moving from electron to hole-dominated states.

An important consideration at this point is whether this shift is rigid or not. The energy shift of the valence band is determined by matching MDCs at different temperatures, correcting the energy to match the one obtained at high temperature (120 K). Horizontal lines in panel (a) show the binding energies at which the MDC peak positions match each other at different temperatures. Plotting these shifts, along with the ones of the core levels in Fig. 5(d), we can see that while the two core levels move rigidly, the energy shift of the valence band is systematically higher for all the temperatures. This indicates that the observed effect cannot be described by only a rigid shift but would require the consideration of a slight change in bandwidth.

III. DISCUSSION

Differences between the ARPES and thermoelectric transport results can, to a certain extent, be explained by surface versus bulk sensitivity [48]. However, if we limit ourselves to a simple EL (HL) conduction (valence) band model, the trend between ARPES and thermopower with temperature dependence is opposite. Moreover, a simply empirical two-band model cannot explain consistently the magnetic field

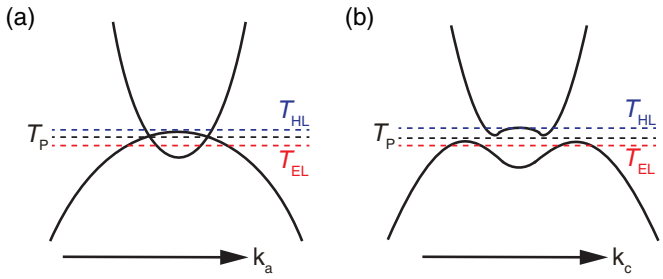

FIG. 6. (a) Schematic band diagram along k_a (X-Γ-X). (b) Schematic band diagram along k_c (Y-Γ-Y). The blue curve, black curve, and red curve represent the temperature above (T_{HL}), at, and below (T_{EL}) the transition temperature T_p, respectively.

dependence of our thermoelectric transport results. Thus, a more complex band model with partially inverted conduction and valence bands would be necessary.

Here, combining our transport and ARPES measurements, we propose a nontrivial band model (Fig. 6) to give a qualitative interpretation to our data. The symmetry protected band crossings in combination with the strong spin-orbit interaction cause the formation of (bulk) Dirac cones, which indicates that $HfTe_5$ would be a Dirac semimetal. The temperature induced movement of the chemical potential can no longer be simply described as a Fermi level shift from conduction (valence) band to valence (conduction) band with increasing temperature. Instead, the Fermi level cuts both the valence and conduction bands in a certain temperature range. Furthermore, by applying a magnetic field, the symmetry is broken and the band gap opens a little bit more, providing an enhanced Berry curvature. This is consistent with the anomalous large Nernst coefficient when a magnetic field is applied, which hints at a strong contribution from the Berry curvature. Additionally, the resistance peak anomaly [see Fig. S3(a)], large anomalous Hall effect [Fig. S3(b)], and negative LMR [Figs. S3(e) and S3(f)] could also provide strong supports for this complex band model.

IV. CONCLUSION

In summary, we performed thermopower and Nernst effect measurements as a function of magnetic field on bulk 3D $HfTe_5$ single crystals. The largest magnetothermopower is observed when the field is applied perpendicular to the layer plane. A large in-plane magnetothermopower is also observed, which is very likely induced by the chiral anomaly that appears around the transition temperature when the conductance changes from electronlike to holelike. A steplike anomalous Nernst effect is clearly observed in our $HfTe_5$ single crystals with a small saturation field of 0.18 T; the sign of the Nernst coefficient changes around the transition temperature at which the Seebeck coefficient also changes sign. Furthermore, large Nernst coefficients, two orders of magnitude larger than the typical values obtained in ferromagnets, are observed in the temperature range from 70 K to 130 K. A simple two-band model cannot describe appropriately the thermoelectric properties observed, nor the electric transport effects. The transport results, supported by our ARPES measurements, indicate that an inverted nontrivial band structure might possible exist in $HfTe_5$. The observed large magnetothermopower, Nernst effect, and their temperature dependence may open up new possibilities in designing thermopile devices (Fig. S8), provide a challenging set of data for any detailed model of transport in $HfTe_5$, and point to the value of further investigating topology-related thermoelectric effects.

ACKNOWLEDGMENTS

We thank Q. Wu, S. Zhang, W.H. Bi, J.Z. Ma, Y. Yao, and F. Levy for helpful discussions. We wish to acknowledge the support by National Natural Science Foundation of China under Grants No. 11674020, and No. U1801661, by the Sino-Swiss Science and Technology Cooperation (SSSTC, Grant No. EG 01-122016) for J.H., by the Program of Introducing Talents of Discipline to Universities in China 111 Program No. B16001 and by the National Key Research and Development Program of China (254).

[1] M. Z. Hasan and C. L. Kane, Rev. Mod. Phys. **82**, 3045 (2010).
[2] Y. Fan and K. L. Wang, Spin **06**, 1640001 (2016).
[3] S.-Y. Xu, I. Belopolski, N. Alidoust, M. Neupane, G. Bian, C. Zhang, R. Sankar, G. Chang, Z. Yuan, C.-C. Lee, S.-M. Huang, H. Zheng, J. Ma, D. S. Sanchez, B. Wang, A. Bansil, F. Chou, P. P. Shibayev, H. Lin, S. Jia, and M. Z. Hasan, Science **349**, 613 (2015).
[4] B. Q. Lv, H. M. Weng, B. B. Fu, X. P. Wang, H. Miao, J. Ma, P. Richard, X. C. Huang, L. X. Zhao, G. F. Chen, Z. Fang, X. Dai, T. Qian, and H. Ding, Phys. Rev. X **5**, 031013 (2015).
[5] Z. Jia, C. Li, X. Li, J. Shi, Z. Liao, D. Yu, and X. Wu, Nat. Commun. **7**, 13013 (2016).
[6] T. Liang, J. Lin, Q. Gibson, T. Gao, M. Hirschberger, M. Liu, R. J. Cava, and N. P. Ong, Phys. Rev. Lett. **118**, 136601 (2017).
[7] Z. Wang, Y. Sun, X.-Q. Chen, C. Franchini, G. Xu, H. Weng, X. Dai, and Z. Fang, Phys. Rev. B **85**, 195320 (2012).
[8] Z. K. Liu, B. Zhou, Y. Zhang, Z. J. Wang, H. M. Weng, D. Prabhakaran, S.-K. Mo, Z. X. Shen, Z. Fang, X. Dai, Z. Hussain, and Y. L. Chen, Science **343**, 864 (2014).
[9] A. A. Burkov, Phys. Rev. Lett. **113**, 247203 (2014).
[10] Q. Li, D. E. Kharzeev, C. Zhang, Y. Huang, I. Pletikosic, A. V. Fedorov, R. D. Zhong, J. A. Schneeloch, G. D. Gu, and T. Valla, Nat. Phys. **12**, 550 (2016).
[11] Z. Song and X. Dai, Phys. Rev. X **9**, 021053 (2019).
[12] J. Xiang, S. Hu, Z. Song, M. Lv, J. Zhang, L. Zhao, W. Li, Z. Chen, S. Zhang, J. Wang, Y. Yang, X. Dai, F. Steglich, G. Chen, and P. Sun, Phys. Rev. X **9**, 031036 (2019).
[13] C. Schindler, S. Galeski, S. N. Guin, W. Schnelle, N. Kumar, C. Fu, H. Borrmann, C. Shekhar, Y. Zhang, Y. Sun, C. Felser, T. Meng, A. G. Grushin, and J. Gooth, arXiv:1810.02300.
[14] S. Furuseth, L. Brattas, and A. Kjekshus, Acta Chem. Scand. **27**, 2367 (1973).
[15] G. Manzoni, L. Gragnaniello, G. Autes, T. Kuhn, A. Sterzi, F. Cilento, M. Zacchigna, V. Enenkel, I. Vobornik, L. Barba, F. Bisti, Ph. Bugnon, A. Magrez, V. N. Strocov, H. Berger, O. V. Yazyev, M. Fonin, F. Parmigiani, and A. Crepaldi, Phys. Rev. Lett. **117**, 237601 (2016).

[16] F. J. DiSalvo, R. M. Fleming, and J. V. Waszczak, Phys. Rev. B **24**, 2935 (1981).
[17] Y. Zhang, C. Wang, G. Liu, A. Liang, L. Zhao, J. Huang, Q. Gao, B. Shen, J. Liu, C. Hu, W. Zhao, G. Chen, X. Jia, L. Yu, L. Zhao, S. He, F. Zhang, S. Zhang, F. Yang, Z. Wang, Q. Peng, Z. Xu, C. Chen, and X. Zhou, Sci. Bull. **62**, 950 (2017).
[18] T. E. Jones, W. W. Fuller, T. J. Wieting, and F. Levy, Solid State Commun. **42**, 793 (1982).
[19] N. Kumar, C. Shekhar, M. Wang, Y. Chen, H. Borrmann, and C. Felser, Phys. Rev. B **95**, 155128 (2017).
[20] L.-X. Zhao, X.-C. Huang, Y.-J. Long, D. Chen, H. Liang, Z.-H. Yang, M.-Q. Xue, Z.-A. Ren, H.-M. Weng, Z. Fang, X. Dai, and G.-F. Chen, Chin. Phys. Lett. **34**, 037102 (2017).
[21] H. Wang, C.-K. Li, H. Liu, J. Yan, J. Wang, J. Liu, Z. Lin, Y. Li, Y. Wang, L. Li, D. Mandrus, X. C. Xie, J. Feng, and J. Wang, Phys. Rev. B **93**, 165127 (2016).
[22] A. C. Niemann, J. Gooth, Y. Sun, F. Thiel, A. Thomas, C. Shekhar, V. Süß, C. Felser, and K. Nielsch, Appl. Phys. Lett. **115**, 072109 (2019).
[23] H. M. Weng, X. Dai, and Z. Fang, Phys. Rev. X **4**, 011002 (2014).
[24] R. Wu, J.-Z. Ma, S.-M. Nie, L.-X. Zhao, X. Huang, J.-X. Yin, B.-B. Fu, P. Richard, G.-F. Chen, Z. Fang, X. Dai, H.-M. Weng, T. Qian, H. Ding, and S. H. Pan, Phys. Rev. X **6**, 021017 (2016).
[25] S. Liu, M. X. Wang, C. Chen, X. Xu, J. Jiang, L. X. Yang, H. F. Yang, Y. Y. Lv, J. Zhou, Y. B. Chen, and S. H. Yao, M. H. Lu, Y. F. Chen, C. Felser, B. H. Yan, Z. K. Liu, and Y. L. Chen, APL Mater. **6**, 121111 (2018).
[26] T. Liang, J. Lin, Q. Gibson, S. Kushwaha, M. Liu, W. Wang, H. Xiong, J. A. Sobota, M. Hashimoto, P. S. Kirchmann, Z.-X. Shen, R. J. Cava, and N. P. Ong, Nat. Phys. **14**, 451 (2018).
[27] S. M. Wu, A. Luican-Mayer, and A. Bhattacharya, Appl. Phys. Lett. **111**, 223109 (2017).
[28] W. Koshibae, K. Tsutsui, and S. Maekawa, Phys. Rev. B **62**, 6869 (2000).
[29] S. J. Watzman, T. M. McCormick, C. Shekhar, S.-C. Wu, Y. Sun, A. Prakash, C. Felser, N. Trivedi, and J. P. Heremans Phys. Rev. B **97** 161404(R) (2018).
[30] J. Niu, J. Wang, Z. He, C. Zhang, X. Li, T. Cai, X. Ma, S. Jia, D. Yu, and X. Wu, Phys. Rev. B **95**, 035420 (2017).
[31] E. Martino, I. Crassee, G. Eguchi, D. Santos-Cottin, R. D. Zhong, G. D. Gu, H. Berger, Z. Rukelj, M. Orlita, C. C. Homes, and A. Akrap, Phys. Rev. Lett. **122**, 217402 (2019).
[32] See Supplemental Material at http://link.aps.org/supplemental/10.1103/PhysRevB.100.115201 for sample information and measurement systems (electric, thermoelectric transport and ARPES); further sample characterization by electric transport properties (magnetoresistance and Hall effect) and thermoelectric transport properties (angle-dependent magnetothermopower, high field magnetothermopower and Nernst effect); two-dimensional band structure of $HfTe_5$; thermopile measurements based on the $HfTe_5$.
[33] Z. M. Gibbs, H.-S. Kim, H. Wang, and G. J. Snyder, Appl. Phys. Lett. **106**, 022112 (2015).
[34] L. Piraux, A. Fert, P. A. Schroeder, R. Loloee, and P. Etienne, J. Magn. Magn. Mater. **110**, L247 (1992).
[35] D. Xiao, Y. Yao, Z. Fang, and Q. Niu, Phys. Rev. Lett. **97**, 026603 (2006).
[36] Y. Pu, D. Chiba, F. Matsukura, H. Ohno, and J. Shi, Phys. Rev. Lett. **101**, 117208 (2008).
[37] R. Mark, Phys. Rev. B **60**, 1627 (1999).
[38] T. Liang, Q. Gibson, M. N. Ali, M. Liu, R. J. Cava, and N. P. Ong, Nat. Mater. **14**, 280 (2014).
[39] X. Huang, L. Zhao, Y. Long, P. Wang, D. Chen, Z. Yang, H. Liang, M. Xue, H. Weng, Z. Fang, X. Dai, and G. Chen, Phys. Rev. X **5**, 031023 (2015).
[40] R. Lundgren, P. Laurell, and G. A. Fiete, Phys. Rev. B **90**, 165115 (2014).
[41] G. Sharma, P. Goswami, and S. Tewari, Phys. Rev. B **93**, 035116 (2016).
[42] S. Tu, J. Hu, G. Yu, H. Yu, C. Liu, F. Heimbach, X. Wang, J. Zhang, A. Hamzić, K. L. Wang, W. Zhao, and J.-P. Ansermet, Appl. Phys. Lett. **111**, 222401 (2017).
[43] G. Sharma, C. Moore, S. Saha, and S. Tewari, Phys. Rev. B **96**, 195119 (2017).
[44] J. M. Ziman, *Electrons and Phonons* (Clarendon Press, Oxford, 1960).
[45] N. W. Ashcroft and N. D. Mermin, *Solid State Physics* (Holt, Rinehart and Winston, New York, 1976).
[46] Y.-Y. Lv, X. Li, L. Cao, D. Lin, S.-H. Yao, S.-S. Chen, S.-T. Dong, J. Zhou, Y. B. Chen, and Y.-F. Chen, Phys. Rev. Applied **9**, 054049 (2018).
[47] P. Shahi, D. J. Singh, J. P. Sun, L. X. Zhao, G. F. Chen, Y. Y. Lv, J. Li, J.-Q. Yan, D. G. Mandrus, and J.-G. Cheng, Phys. Rev. X **8**, 021055 (2018).
[48] S. Muff, F. von Rohr, G. Landolt, B. Slomski, A. Schilling, R. J. Cava, J. Osterwalder, and J. H. Dil, Phys. Rev. B **88**, 035407 (2013).